International Journal of Computer Assisted Radiology and Surgery (2022) 17:589–600
https://doi.org/10.1007/s11548-022-02566-7

ORIGINAL ARTICLE

Brain tumor segmentation in MRI images using nonparametric localization and enhancement methods with U-net

Ahmet Ilhan[1] · **Boran Sekeroglu**[1] · **Rahib Abiyev**[1]

Received: 18 August 2021 / Accepted: 12 January 2022 / Published online: 29 January 2022

Abstract

Purpose: Segmentation is one of the critical steps in analyzing medical images since it provides meaningful information for the diagnosis, monitoring, and treatment of brain tumors. In recent years, several artificial intelligence-based systems have been developed to perform this task accurately. However, the unobtrusive or low-contrast occurrence of some tumors and similarities to healthy brain tissues make the segmentation task challenging. These yielded researchers to develop new methods for preprocessing the images and improving their segmentation abilities.

Methods: This study proposes an efficient system for the segmentation of the complete brain tumors from MRI images based on tumor localization and enhancement methods with a deep learning architecture named U-net. Initially, the histogram-based nonparametric tumor localization method is applied to localize the tumorous regions and the proposed tumor enhancement method is used to modify the localized regions to increase the visual appearance of indistinct or low-contrast tumors. The resultant images are fed to the original U-net architecture to segment the complete brain tumors.

Results: The performance of the proposed tumor localization and enhancement methods with the U-net is tested on benchmark datasets, BRATS 2012, BRATS 2019, and BRATS 2020, and achieved superior results as 0.94, 0.85, 0.87, 0.88 dice scores for the BRATS 2012 HGG-LGG, BRATS 2019, and BRATS 2020 datasets, respectively.

Conclusion: The results and comparisons showed how the proposed methods improve the segmentation ability of the deep learning models and provide high-accuracy and low-cost segmentation of complete brain tumors in MRI images. The results might yield the implementation of the proposed methods in segmentation tasks of different medical fields.

Keywords Brain tumor · Segmentation · MRI · Tumor localization · Tumor enhancement · U-net

Introduction

A brain tumor is the mass of abnormal cells that grows uncontrollably in the brain. Tumors that are characterized by cancerous and non-cancerous brain cells are classified as malignant and benign. Contrary to the benign tumors' inactive cells content and uniform structure, malignant tumors occur in a non-uniform structure containing active cells. In recent years, radiologists frequently predicted gliomas that occur in the glial cells or the spinal cord, and categorized as high-grade (HGG) and low-grade gliomas (LGG), according to the prevalences and high mortality rates [1,2].

Magnetic resonance imaging (MRI) is common for obtaining multimodal images and showing brain structures in detail. Brain MRI images consist of four modalities (T1, T1c, T2, and FLAIR), and all of these modalities are available in the sagittal, coronal, and axial planes [3]. Healthy brain tissues are analyzed using T1 images when contrast enhancement by intravenous application of gadolinium is not used. T1c images are used in a similar way; however, tumor borders are highlighted in these images. The images with the highest intensities are obtained in the T2 images because of the fluids, including tumor edema. Finally, FLAIR images attenuate the cerebral fluid and determine the abnormality area [4]. Even though each modality has a unique representation

Boran Sekeroglu and Rahib Abiyev have contributed equally to this work.

✉ Ahmet Ilhan
ahmet.ilhan@neu.edu.tr

Boran Sekeroglu
boran.sekeroglu@neu.edu.tr

Rahib Abiyev
rahib.abiyev@neu.edu.tr

[1] Computer Engineering Department, Near East University, 99138 Nicosia, Cyprus, TR, Mersin 10, Turkey

and process, FLAIR is the most suitable one for segmenting the tumorous region because of provided abnormality area.

Segmenting brain tumors using MRI images is challenging and time-consuming because of the complex structure of tumors, which differs in size, shape, location, and appearance [5]. Therefore, the segmentation of brain tumors are of great importance. Various methods, such as thresholding [6], region growing [7], and clustering [8], were proposed and implemented for this purpose. Artificial intelligence (AI), machine learning (ML), and particularly deep learning (DL) architectures have recently been implemented for segmenting brain tumors due to their reasonable decisions and results.

Rehman et al. [9] proposed a system to segment the brain tumors. Initially, filtering approaches was applied to the images. Then, the images were segmented out into superpixel, and low-level features were extracted using intensity features and histogram level of texton-map. A leave-one-out cross-validation (LOOCV) was applied at the final stage to classify the image pixels in BRATS 2012 dataset as tumorous and non-tumorous using several ML classifiers. The performance of the random forest was reported as superior.

Amin et al. [10] proposed a system consisting of filtering and clustering approaches to detect tumors. Finally, the tumorous region was isolated using global thresholding and additional morphological operations. The system was tested on BRATS 2013, BRATS 2015, and self-made datasets. Soltaninejad et al. [11] partitioned the images into patches using the superpixel technique. Statistical, texton, and shape features were extracted for each superpixel patch and the feature selection was applied. SVM and extremely randomized trees (ERT) classifiers were used to classify the pixels as tumorous or non-tumorous. The system was tested on BRATS 2012 dataset, and the performance of the ERT was reported as superior to the SVM.

The efficiency of convolutional neural networks (CNN) in segmentation tasks has gained significant importance with the development of deep architectures. CNN has its own feature extraction, representation, and learning processes that improve the rates obtained by traditional machine learning algorithms. For that reason, several kinds of research were performed based on CNN and particularly the U-net for segmenting multi-class and complete brain tumors. [12–15].

Razzak et al. [16] proposed a two-pathway-group CNN architecture that incorporates images' local and global contextual features to segment the brain tumors and tested it on BRATS 2015 dataset. Li et al. [17] proposed a modified U-net [18] architecture to perform end-to-end brain tumor segmentation. The system was tested on BRATS 2015 and BRATS 2016 datasets.

Hu et al. [19] used fully connected conditional random fields that smooth the tumors' edges and eliminate false positives based on multi-cascade CNN for brain tumor segmentation and tested it on BRATS 2013, BRATS 2015, and BRATS 2018 datasets. Khan et al. [20] proposed a cascading method that combines handcrafted features and CNN to segment the brain tumors. The method was tested on BRATS 2015 dataset.

Wu et al. [21] proposed a combined architecture named deep convolutional neural network fusion support vector machine (DCNN-F-SVM) to segment the brain tumors in BRATS 2018 and self-made datasets. Chithra et al. [22] proposed a CNN architecture based on Di-phase midway for the brain tumor segmentation. The architecture was tested on BRATS 2012, BRATS 2013, and BRATS 2018 datasets.

Zeineldin et al. [23] proposed a combined architecture named DeepSeg for brain tumor segmentation. The architecture was based on U-net; however, the encoder part of the modified U-net architecture was rearranged using several deep learning architectures (i.e., [24–28]). The architecture was tested on BRATS 2019 dataset.

Sohail et al. [29] proposed a 3D U-net architecture to segment the brain tumors and tested it on BRATS 2019 and BRATS 2020 datasets. Saeed et al. [30] proposed a combined architecture named RMU-net to segment the brain tumors. In the encoder part of the architecture, modified MobileNetV2 [31] was used and combined with the U-net decoder. The architecture was tested on BRATS 2018, BRATS 2019, and BRATS 2020 datasets.

The above-mentioned studies and performed researches have proposed and implemented different methods to achieve the highest success rate and minimum error for the complete brain tumor segmentation. The segmentation of the complete brain tumors is considered an essential step in differentiating sub-classes (core and enhancing tumor), and this increases the importance of the achievements and ensures that the studies also continue in this direction.

The supervised feature extraction ability of the deep learning architectures, particularly the U-net model, provides effective segmentation of medical images and leads to new models or modifying existing ones by combining the models or adding or removing some blocks. Additionally, the positive effect of proper preprocessing of images on the success of neural networks has also been proven in many different problem domains [32,33]. Therefore, combining the unique abilities of the deep learning models with the particularly developed preprocessing approaches for the images would provide high accurate segmentation of the brain tumors.

This study proposes a brain tumor segmentation system based on nonparametric tumor localization and enhancement methods and U-net architecture. The proposed system segments the brain tumors using the 2D axial images obtained from the patients' FLAIR modalities. The proposed methods are performed to improve the ability of deep learning architectures in feature extraction and segmentation. The resultant images obtained from the proposed preprocessing methods

are fed to the original U-net architecture, and complete brain tumors are segmented with a high success rate.

Materials and methods

Dataset

This study considered three common and recent BRATS [3, 34–37] datasets (BRATS 2012, BRATS 2019, and BRATS 2020) to evaluate the proposed system.

BRATS 2012 is the most commonly used dataset for the complete brain tumor segmentation task [8,9,11,22] and consisted of 30 patients as 20 HGG and 10 LGG. The total number of 2D FLAIR axial images (tumorous and non-tumorous) of the HGG and LGG patients is 3,725 and 1,908, respectively.

One of the recent versions of the BRATS datasets is 2019 and consisted of 335 patients as 259 HGG and 76 LGG. The total number of 2D FLAIR axial images (tumorous and non-tumorous) of the HGG and LGG patients is 40,145 and 11,780, respectively.

The final version of the BRATS dataset was released in 2020 and consisted of 369 patients. The total number of 2D FLAIR axial images (tumorous and non-tumorous) of the patients is 57,195.

Each image in the BRATS datasets contains four modalities as T1, T1c, T2, and FLAIR. The images are skull stripped and the experienced radiologists annotated their ground truths.

The proposed system

Initially, all tumorous images are filtered using a 5x5 mean filer to remove noise [38]. Then, nonparametric tumor localization and enhancement methods are applied to localize and clarify the tumorous regions and provide a more effective segmentation process. Finally, the original U-net architecture is used to perform the segmentation of the tumors using the resultant images.

Proposed tumor localization and enhancement methods

In the first step of the proposed tumor localization method, the background and tumorous regions are determined using the image histogram, which provides the frequency distribution of the intensity values in the image [39]. Zero intensity values are excluded from the obtained image histogram to eliminate the slices' background and frame, and the frequency of each intensity value is calculated as shown in Eq. 1:

$$n_j = \sum_{j=1}^{k-1} I_j \quad \text{and} \quad I(x, y) \in [0, k-1] \tag{1}$$

where j is the range between 1 and maximum intensity range within the image $k-1$, n_j is the histogram value of j^{th} intensity value of the image, I_j is the image and x and y are the spatial coordinates of the image.

The second step of the proposed method is to determine the initial nonparametric threshold value θ_{fr} using frequencies of the intensity values obtained by the image histogram in order to optimize the determination of background, irrelevant, and the most informative regions within the image while the most frequent intensity values in brain MRI images represent the healthy brain tissues and tumorous region. The θ_{fr}, which can be described as the mean of intensity frequencies, is calculated as shown in Eq. 2.

$$\theta_{\text{fr}} = \frac{1}{k-1} \sum_{j=1}^{k-1} n_j \tag{2}$$

Since all tumors do not appear significantly in the MRI images, the following steps of the proposed method aim to determine the tumor region as a significant or low-contrast tumor to provide robust enhancement before the segmentation process.

The θ_{fr} is used to determine the $B_{\min}$ and $T_{\min}$ values that represent the minimum values for the background and tumorous regions using Eq. 3:

$$B_{\min} = \min(I_{\theta_{fr}}) \quad \text{and} \quad T_{\min} = \max(I_{\theta_{fr}}) \tag{3}$$

where $I_{\theta_{\text{fr}}}$ is the intensity values where the frequencies are more than θ_{fr}.

The calculation of $B_{\min}$ and $T_{\min}$ provided us to initially localize the tumorous region, where $B_{\min} < T_{\min}$ is the background and $T_{\min} < k-1$ is the tumorous region.

We hypothesize that if the tumorous region's standard deviation is higher than the standard deviation of the background region, the tumor could easily be distinguished and segmented. Otherwise, the localization of background and tumorous regions requires further processing since the low-contrast appearance of brain tumors that are not significantly distinguishable from the healthy brain tissues. Therefore, fundamental statistical approach, standard deviation [40], is used to determine the distinguishability and contrast between the background and tumorous regions. The standard deviations of the background and tumorous regions are calculated

using Eq. 4:

$$\mathrm{Std}_j = \sqrt{\frac{\sum (I_{ij} - m_j)^2}{n_j}} \tag{4}$$

where I_i, m, and n represent intensity value, mean value, and the number of pixels belonging to the region j which is background (B) or tumorous (T).

After the initial localization and the determination of the contrast level of the tumor, we propose a tumor enhancement method that significantly increases the visual appearance of the tumorous region even it is low-contrast or not.

Our enhancement method and final localization are based on the conditions after comparing the standard deviations obtained for both background and tumorous regions. Similar to our hypothesis mentioned above, the tumor is localized in the initial background region if the background region's standard deviation is higher than the initial tumorous region. Otherwise, it is localized in the initial tumorous region. The formula of final localization is given in Eq. (5):

$$\begin{cases} B & \text{if } \mathrm{Std}_B > \mathrm{Std}_T \\ T & \text{if } \mathrm{Std}_B < \mathrm{Std}_T \end{cases} \tag{5}$$

where B and T denote the background and tumorous regions, respectively.

After the final localization, the proposed enhancement method is applied to the localized tumorous region and ignored the empty region to make the tumorous region more significant. Our enhancement method uses two stages for low-contrast and distinguishable tumors according to the localized regions. First, it considers the minimum value and the standard deviation of the tumorous region to make the intensity values of the tumor more significant if the tumor is localized in the T region, as shown in Eq. (6).

$$O_T = \frac{I_{T(x,y)} - T_{\min}}{\mathrm{Std}_T} \tag{6}$$

However, our proposed enhancement method considers the updated minimum value for the tumorous region and the updated standard deviation to make the low-contrast tumor more significant if the tumor is localized in the B region. The formula of updated tumorous region $T_{U_{\min}}$ and Std_{T_U} is shown in Eqs. 7 and 8.

$$T_{U_{\min}} = \frac{1}{x} \sum_{j=B_{\min}}^{k-1} I_j \tag{7}$$

where $T_{U_m in}$ is the updated minimum value of the tumorous region and is defined as the mean intensity values between B_{min} and $k-1$, and x represents the pixel within the region.

$$\mathrm{Std}_{T_U} = \sqrt{\frac{\sum (I_{iT_U} - m_{T_U})^2}{n_{T_U}}} \tag{8}$$

where I_{iT_U}, m_{T_U}, and n_{T_U} represent intensity value, mean value, and the number of pixels belonging to the updated tumorous region ($T_{U_{\min}}$). Therefore, the final enhancement for the low-contrast and indistinct tumorous region is calculated as given below in Eq.(9).

$$O_B = \frac{I_{T(x,y)} - T_{U_{\min}}}{\mathrm{Std}_{T_U}} \tag{9}$$

Finally, the enhanced image is added to the initially filtered one, and the resultant image O_R is obtained to be fed to the U-net architecture, as shown in Eq. (10).

$$O_R = I_f + O_i \tag{10}$$

where I_f denotes the filtered image and O_i is defined as O_T or O_B according to Eq. (5).

Figure 1 demonstrates the determined background and tumorous regions on sample images (with minimum values) using the proposed tumor localization method and their corresponding standard deviations and the resultant images. Similarly, the 3rd row demonstrates the localization and enhancement of the tumorous region; however, it is clearly seen that in some images, similar components of the brain that have close intensity values with tumorous regions are also localized and enhanced, and this makes the use of supervised segmentation techniques compulsory, such as the U-net, instead of thresholding, region growing or clustering methods, to avoid the segmentation of irrelevant regions.

U-net architecture

We used the original U-net architecture to segment the complete brain tumors following the proposed tumor localization and enhancement methods. The U-net [18] was developed to provide efficient segmentation of biomedical images.

The U-net architecture consists of two paths named contraction and expansion. The contraction path (encoder) consists of a series of blocks and each block includes two 3x3 convolution layers, each followed by a rectified linear unit (ReLU), and a 2x2 maximum pooling operation with stride 2. After each block, the number of feature maps is doubled, thus enabling the architecture to learn complex structures more effectively.

The expansion path (decoder) has a similar design to the contraction path. Each block contains a 2x2 up-convolution layer, and two 3x3 convolution layers, each followed by a ReLU. At the end of each block, the number of feature maps

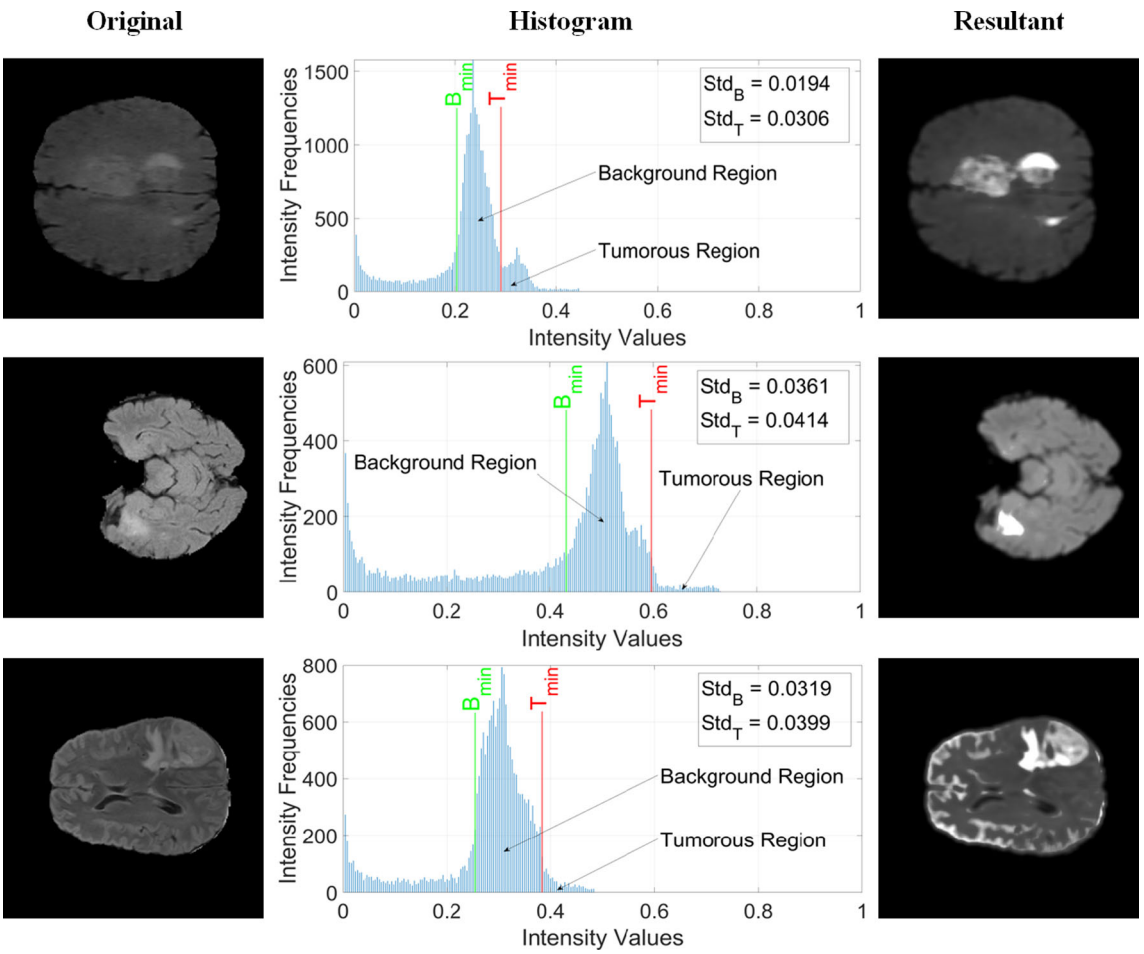

Fig. 1 Visualization of the proposed tumor localization and enhancement methods

is halved to maintain symmetry. However, the feature map of each up-convolution layer is concatenated with the cropped feature map of the corresponding contraction layer. Cropping is required because of the loss of border pixels at each convolution operation.

Finally, pass through a 1x1 convolution layer with a number of feature maps equal to the desired number of classes, and then pixel-wise softmax activation and cross-entropy loss functions are applied to the resultant feature map. In this way, each pixel in the image is classified as belonging to a class.

Results and comparisons

This section presents the obtained results, statistical tests, and comparisons performed in this study. The experiments are based on the training sets of the considered datasets to demonstrate the effect of the localization and enhancement methods.

In this study, several experiments are performed to evaluate the performance of the proposed system. Furthermore, the initial experiments on the validation set of the BRATS2020 are also performed to demonstrate the positive effect of the proposed methods on the deep segmentation models. We used six metrics: accuracy, sensitivity, specificity, precision, dice score, and Jaccard index to evaluate the performance of the proposed system [41,42]. In addition to the common evaluation metrics, a statistical significance test is performed, and the Matthews correlation coefficient (MCC) [42], which is used to measure the correlation between the segmented mass pixels and corresponding ground truths, is determined for each dataset.

In the first experiment, the HGG images of the BRATS 2012 dataset are trained using the fivefold cross-validation [43]. The training parameters are determined as 0.001, 50, and 8 for the learning rate, the number of epochs, and batch size, respectively. The proposed system achieved the mean accuracy, sensitivity, specificity, precision, dice score, and Jaccard index as 99.38%, 92.19%, 99.75%, 95.04%, 0.94, and 0.88 in this experiment.

In the second experiment, the LGG images of the BRATS 2012 dataset are tested using the network that achieved the

Table 1 Obtained results by the proposed system for training data

Dataset	Acc (%)	Sens (%)	Spec (%)	Prec (%)	Dice	Jaccard
BRATS 2012 HGG	99.38	92.19	99.75	95.04	0.94	0.88
BRATS 2012 LGG*	99.12	83.27	99.62	87.18	0.85	0.74
BRATS 2019	99.38	83.01	99.82	92.60	0.87	0.78
BRATS 2020	99.40	83.62	99.83	92.94	0.88	0.79

*:untrained, ACC: accuracy, Sens: sensitivity, Spec: specificity, Prec: precision

Table 2 Dice measurements of the proposed system for training and validation sets

	BRATS2012 HGG	BRATS2012 LGG (untrained)	BRATS 2019	BRATS2020 Training
Mean	0.94	0.85	0.87	0.88
Median	0.96	0.87	0.90	0.91
StdDev	0.19	0.27	0.32	0.32
25quantile	0.88	0.72	0.67	0.70
75quantile	0.97	0.92	0.93	0.93
	BRATS2020 Validation (Proposed System)		BRATS2020 Validation (U-Net)	
Mean	0.81		0.77	
Median	0.87		0.83	
StdDev	0.17		0.16	
25quantile	0.80		0.70	
75quantile	0.91		0.88	

highest success rate in the first experiment without training any LGG images. The LGG images are resized as 240x240 and preprocessed using the proposed tumor localization and enhancement methods. Then, the preprocessed images are tested using the trained network that achieved the highest dice score and Jaccard index in the first experiment folds. The segmentation of LGG images without training achieved 99.12% accuracy, 83.27% sensitivity, 99.62% specificity, 87.18% precision, 0.85 dice score, and 0.74 Jaccard index.

In the third experiment, the BRATS 2019 dataset is trained without distinguishing HGG-LGG using the fivefold cross-validation as in the first experiment. The training parameters are determined as 0.001, 10, and 8 for the learning rate, the number of epochs, and batch size, respectively. The proposed system achieved the mean accuracy, sensitivity, specificity, precision, dice score, and Jaccard index as 99.38%, 83.01%, 99.82%, 92.60%, 0.87, and 0.78, respectively.

Similar to the BRATS 2019 dataset, BRATS 2020 is trained in the study's final experiment without distinguishing HGG-LGG using the fivefold cross-validation, and the training parameters are set as same as the BRATS 2019 U-net architecture. The proposed system achieved the mean accuracy, sensitivity, specificity, precision, dice score, and Jaccard index as 99.40%, 83.63%, 99.83%, 92.94%, 0.88, and 0.79, respectively. In addition, the proposed system is used to compare the results with the original U-Net using the BRATS2020 validation set. The U-Net with the proposed localization and enhancement methods obtained an 0.81 dice score for complete tumor for the validation set (results obtained from BRATS organizers online evaluation platform); however, the U-Net without the proposed methods obtained 0.77. Tables 1 and 2 present all the results obtained by the proposed system and the dice measurements of the proposed method, respectively. Figure 2 shows the segmentation results, including a sample for each experiment.

The proposed system is compared with the recent studies that focused on the complete brain tumor segmentation task. Tables 3 and 4 show the comparison results of the proposed system for the BRATS 2012 and BRATS 2019-BRATS 2020 datasets.

Figure 3 shows the visualization of the comparative segmentation results. It is clear that the all of the proposed methods in the literature are capable of segmenting complete brain tumors; however, the details localized and enhanced by our proposed methods create differences within other methods and the produced results.

The average tumor volume is calculated for each dataset. The volumes are obtained using the number of tumor voxels multiplied by the voxel volume [44] and converted to cm^3 after calculating the average of all slices. Then, the correctly segmented tumor volumes are calculated and compared to the actual values to observe the agreement. The agreement between the tumor volume extracted on the ground-truth images and the proposed methods is calculated as 92.22%, 83.48%, 83.01%, and 83.57% for BRATS 2012 HGG, LGG, BRATS 2019, and BRATS 2020 datasets. In addition, the

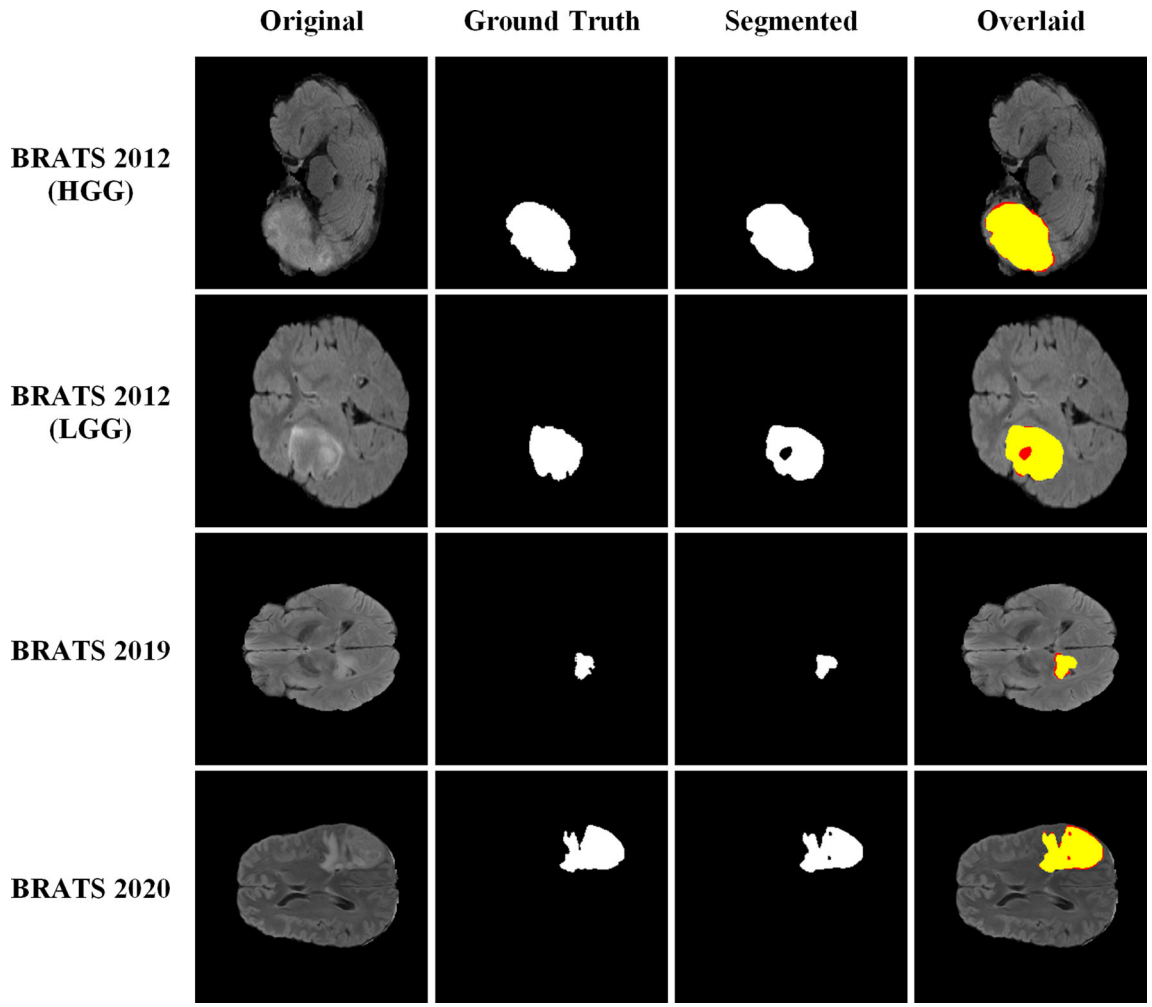

Fig. 2 Sample segmentation results of the proposed system: The red and yellow regions in the overlaid images represent the ground truth and segmented tumor, respectively

Table 3 Comparison of the results for complete tumor segmentation for BRATS2012

BRATS 2012 Study	Tumor Type	Method	Dice
-	HGG	U-Net	0.90
-	LGG (untrained)		0.82
[8]	HGG	K-means clustering with CH cluster validity index	0.89
	LGG		0.84
[9]	HGG	LOOCV and random forest	0.88
	LGG		0.81
[22]	HGG	CNN architecture based on Di-phase midway	0.84
	LGG		**0.85**
Proposed	HGG	Tumor localization and enhancement + U-net	**0.94**
	LGG (untrained)		**0.85**

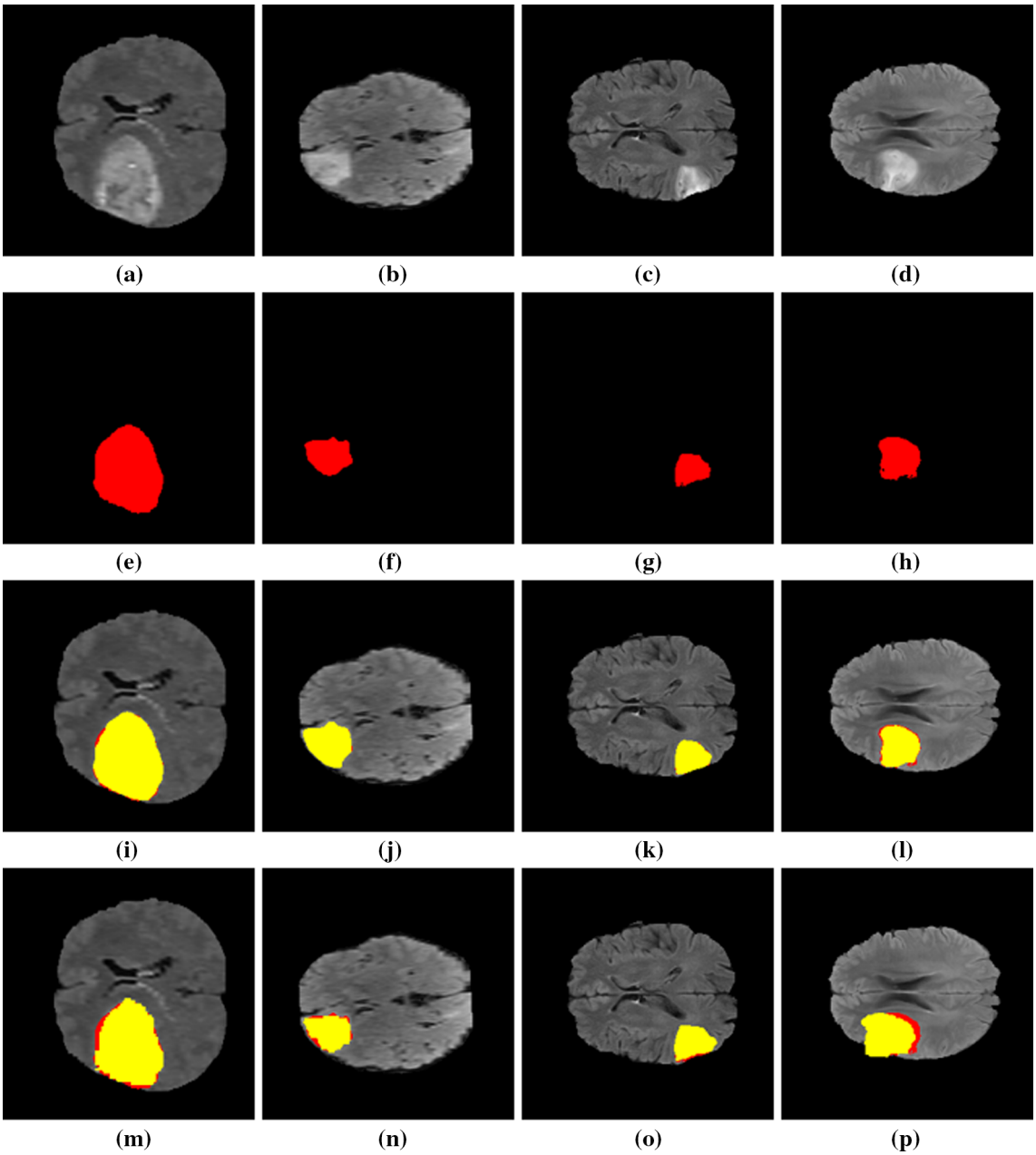

Fig. 3 Comparative segmentation results: **a**–**d** Original images for BRATS2012 HGG, LGG, BRATS2019, and BRATS2020 datasets, respectively; **e**–**h** corresponding ground truth images; **i**–**l** overlaid outputs of proposed system, **m**–**n** [8], **o** [23], and **p** [13]

correlation between the segmented mass pixels and corresponding ground truths is calculated using MCC. The results are shown in Table 5 in detail.

Mann–Whitney U test [45] is performed to test the statistical significance of the methods, and p values are calculated. True positive and true negative results of the segmentation results, which are the main indicators for all evaluation metrics, are considered, and p value is assigned as 0.001 to accept or reject the hypothesis (Table 6). The lower p values show that the results are replicable and have a significant effect. Table 6 shows the p values of the obtained results for the BRATS2012 HGG, LGG, BRATS2019, and BRATS2020 datasets.

Discussions

The lack of distinct tumors in MRI images requires enhancing these regions to provide more accurate segmentation. How-

Table 4 Comparison of the U-net-based models results for complete tumor segmentation for training data of BRATS2019 and BRATS2020

BRATS 2019		
Study	Method	Dice
[23]	U-net	0.81
[23]	Combination of modified U-net and Xception	0.84
[29]	3D U-net	0.78
[12]	ASPP + 3D U-Net	0.86
Proposed	Tumor localization and enhancement + U-net	**0.87**
BRATS 2020		
Study	Method	Dice
-	U-Net	0.85
[29]	3D U-net	0.72
[13]	Basic 3D-UNet	0.85
[13]	Residual 3D-UNet	0.82
[13]	Residual 3D-UNet-multiscale	0.84
[14]	MVP U-Net	0.80
[15]	Multi-threshold Attention U-Net	0.72
Proposed	Tumor localization and enhancement + U-net	0.88
[47]	nnU-net	**0.91**

Table 5 Agreement percentages of actual and segmented tumor volume (cm^3) and MCC results

Dataset	Tumor Vol.	Correctly Segmented Tumor Vol.	Agreement (%)	MCC
BRATS2012 HGG	2.795	2.577	92.22	0.932
BRATS2012 LGG	1.744	1.456	83.48	0.847
BRATS2019	1.495	1.241	83.01	0.872
BRATS2020	1.504	1.257	83.57	0.878

Table 6 p values obtained for true positive and true negative results

BRATS2012 HGG	p value	BRATS2012 LGG	p value
TP	0.0008	TP	4.7×10^{-6}
TN	0.0009	TN	0.0006
BRATS2019	p value	BRATS2020	p value
TP	3.06×10^{-8}	TP	6.14×10^{-7}
TN	7.83×10^{-7}	TN	3.25×10^{-7}

ever, the enhancement of the tumor region initially requires effective localization to apply enhancement only to the region of interest.

The localization of the tumors according to the basic characteristics of the images using a nonparametric localization method enabled us to apply the proposed enhancement method to increase the visual appearances of indistinct tumors. Similarly, the proposed localization and enhancement methods minimize segmentation errors for the distinct tumors that occurred in high-contrast images by adjusting the pixel values similar to the background within the tumorous region. Therefore, indistinct tumorous regions or pixels are clarified, and the background regions are preserved with low computation cost (average processing time/image = 0.0028 sec.).

Due to the nonparametric and automated procedure of the proposed methods, the computational cost is minimized by preventing the selection of any parameters for the images. This also provided more distinguishable tumorous regions and informative features to the original U-net architecture to extract features more efficiently and perform segmentation with highly accurate results. The supervised learning and feature extraction nature of the deep segmentation methods focuses on the regions provided in the ground truths to extract the relevant features and obtain the ability to segment untrained data. The proposed localization and enhancement methods yielded the deep learning model to mainly focus on the enhanced and visually improved tumorous regions by eliminating and not considering irrelevant components. This increased the segmentation results of the U-net by 0.03, 0.03,

0.06, and 0.03 for BRATS2012 HGG, LGG, BRATS2019, and BRATS2020 datasets, respectively. The obtained results showed that the low-cost preprocessing of images significantly increases the segmentation abilities of deep learning models without modifying the internal architecture. On the other hand, datasets are trained without any data augmentation technique and minimize the computational time for the U-net architecture training compared to the other studies [23,46]. In addition to the training set results, validation set results obtained from the BRATS organizers online platform showed that the proposed localization and enhancement methods increased the segmentation ability of the original U-Net architecture (Dice score on BRATS2020 validation set = 0.775) by 3.50% while decreasing the training time and computational cost.

The BRATS 2020 challenge showed that the modifications of deep learning models for brain tumor segmentation had an increasing interest. Different models were proposed to improve the segmentation results, and even though several reasonable results were obtained, the highest mean performance was achieved by nnU-net [47], which was particularly adopted for brain tumor segmentation [46] (WT= 0.9124, for validation set). The main advantage of the nnU-net is the capability of adaptation for different medical image segmentation tasks, which was proved in the BRATS2020 challenge. However, the drawback of the model is the huge computational cost which was mentioned by the authors that five days are required for training (batch = 5) with high-performance computers.

The nnU-net model achieved the highest validation set results for the BRATS2020 dataset using region training and data augmentation with the baseline model. Therefore, the implementation of effective preprocessing methods such as the proposed localization and enhancement might yield an increase in segmentation rates without implementing additional techniques that reduce the cost-effectivity of the model.

In addition, implementing the proposed methods with the recent deep learning models such as H^2NF-Net [48], Modality-Pairing Learning [49], and SA-Net [50] (BRATS2020 Validation Set Complete Tumor Dice Scores: 0.9129, 0.907, and 0.9108, respectively), proposed and developed for BRATS2020, might significantly increase the brain tumor segmentation results and decrease the computational costs mentioned above for further studies.

The limitation of the proposed system is determined on the images consist of multiple indistinct tumorous regions with a few pixels. This is based on the assumption that the tumor is a single region; however, the methods could be modified to detect multiple regions to avoid this limitation in the future.

Another limitation of the study is the consideration of the FLAIR images only for complete tumor segmentation and not testing the proposed methods with other modalities for segmenting tumors as multi-class. Our future work will focus on this subject.

Conclusion

In this study, nonparametric tumor localization and enhancement methods were combined with the original U-net architecture and proposed as a complete brain tumor segmentation system. The proposed system is tested on three benchmark datasets, BRATS 2012 HGG-LGG, BRATS 2019, and BRATS 2020, and the superior segmentation performance is obtained in segmenting complete brain tumors by achieving 0.94, 0.87, and 0.88 dice scores for the considered datasets. In addition, a 0.85 dice score is obtained by the proposed system using the untrained BRATS 2012 LGG dataset.

The results showed that the effective localization and enhancement of tumorous regions yield the deep learning architectures to learn features more effectively and segment the trained or untrained datasets accurately without requiring data augmentation techniques and modifying the deep learning architectures.

The future work will include improving the proposed system to segment sub-classes of brain tumors named core and enhancing tumors after performing complete tumor segmentation.

Funding The authors received no financial support for the research, authorship, and/or publication of this article.

Declarations

Conflict of interest/Competing interests: The authors declare that they have no conflict of interest.

Ethics approval: This article does not contain any studies with human participants or animals performed by any of the authors.

Consent to participate: This article does not contain patient data.

References

1. Pereira S, Pinto A, Alves V, Silva CA (2016) Brain tumor segmentation using convolutional neural networks in MRI images. IEEE Trans Med Imaging 35(5):1240–1251. https://doi.org/10.1109/TMI.2016.2538465
2. Chithra P, Dheepa G (2018) An analysis of segmenting and classifying tumor regions in MRI images using CNN. Int J Pure Appl Math 01(118):1–12
3. Menze BH, Jakab A, Bauer S, Kalpathy-Cramer J, Farahani K, Kirby J, Burren Y, Porz N, Slotboom J, Wiest R, Lanczi L, Gerstner E, Weber MA, Arbel T, Avants BB, Ayache N, Buendia P, Collins DL, Cordier N, Corso JJ, Criminisi A, Das T, Delingette H, Demiralp C, Durst CR, Dojat M, Doyle S, Festa J, Forbes F, Geremia E, Glocker B, Golland P, Guo X, Hamamci A, Iftekharud-

din KM, Jena R, John NM, Konukoglu E, Lashkari D, Mariz JA, Meier R, Pereira S, Precup D, Price SJ, Raviv TR, Reza SMS, Ryan M, Sarikaya D, Schwartz L, Shin HC, Shotton J, Silva C, Sousa N, Subbanna NK, Szekelyand G, Taylor TJ, Thomas OM, Tustison NJ, Unal G, Vasseur F, Wintermark M, Ye DH, Zhao L, Zhao B, Zikic D, Prastawa M, Reyes M, Van Leemput K (2015) The multimodal brain tumor image segmentation benchmark (BRATS). IEEE Trans Med Imaging 34(10):1993–2024. https://doi.org/10.1109/TMI.2014.2377694

4. Currie S, Hoggard N, Craven IJ, Hadjivassiliou M, Wilkinson ID (2013) Understanding MRI: basic MR physics for physicians. Postgrad Med J 89(1050):209–223. https://doi.org/10.1136/postgradmedj-2012-131342
5. Anitha V, Murugavalli S (2016) Brain tumour classification using two-tier classifier with adaptive segmentation technique. IET Comput Vision 10(1):9–17. https://doi.org/10.1049/iet-cvi.2014.0193
6. Rajinikanth V, Satapathy SC, Fernandes SL, Nachiappan S (2017) Entropy based segmentation of tumor from brain MR images - a study with teaching learning based optimization. Pattern Recogn Lett 94:87–95. https://doi.org/10.1016/j.patrec.2017.05.028
7. Kalaiselvi T, Kumarashankar P, Sriramakrishnan P (2020) Three-phase automatic brain tumor diagnosis system using patches based updated run length region growing technique. J Digit Imaging 33:465–479. https://doi.org/10.1007/s10278-019-00276-2
8. Eltayeb E, Salem N, Al-Atabany W (2019) Automated brain tumor segmentation from multi-slices FLAIR MRI images. Bio-Med Mater Eng 08(30):1–13. https://doi.org/10.3233/BME-191066
9. Rehman ZU, Zia MS, Bojja GR, Yaqub M, Jinchao F, Arshid K (2020) Texture based localization of a brain tumor from MR-images by using a machine learning approach. Med Hypotheses. https://doi.org/10.1016/j.mehy.2020.109705
10. Amin J, Sharif M, Raza M, Saba T, Anjum MA (2019) Brain tumor detection using statistical and machine learning method. Comput Methods Programs Biomed 177:69–79. https://doi.org/10.1016/j.cmpb.2019.05.015
11. Soltaninejad M, Yang G, Lambrou T, Allinson N, Jones TL, Barrick TR, Howe FA, Ye X (2017) Automated brain tumour detection and segmentation using superpixel-based extremely randomized trees in FLAIR MRI. Int J CARS 12:183–203. https://doi.org/10.1007/s11548-016-1483-3
12. Ahmad P, Qamar S, Hashemi SR, Shen L (2020) Hybrid labels for brain tumor segmentation. In: Crimi A, Bakas S (eds) Brainlesion: glioma, multiple sclerosis, stroke and traumatic brain injuries. BrainLes 2019. Lecture notes in computer science, vol 11993. Springer, Cham. https://doi.org/10.1007/978-3-030-46643-5_15
13. Ballestar LM, Vilaplana V (2021) MRI brain tumor segmentation and uncertainty estimation using 3D-UNet architectures. In: Crimi A, Bakas S (eds) Brainlesion: glioma, multiple sclerosis, stroke and traumatic brain injuries. BrainLes 2020. Lecture notes in computer science, vol 12658. Springer, Cham. https://doi.org/10.1007/978-3-030-72084-1_34
14. Zhao C, Zhao Z, Zeng Q, Feng Y (2021) MVP U-Net: multi-view pointwise U-net for brain tumor segmentation. In: Crimi A, Bakas S (eds) Brainlesion: glioma, multiple sclerosis, stroke and traumatic brain injuries BrainLes 2020 Lecture notes in computer science, vol 12659. Springer, Cham. https://doi.org/10.1007/978-3-030-72087-2_9
15. Awasthi N, Pardasani R, Gupta S (2021) Multi-threshold Attention U-Net (MTAU) based model for multimodal brain tumor segmentation in MRI scans. In: Crimi A, Bakas S (eds) Brainlesion: glioma, multiple sclerosis, stroke and traumatic brain injuries. BrainLes 2020. Lecture notes in computer science, vol 12659. Springer, Cham. https://doi.org/10.1007/978-3-030-72087-2_15
16. Razzak MI, Imran M, Xu G (2018) Efficient brain tumor segmentation with multiscale two-pathway-group conventional neural networks. IEEE J Biomed Health Inform 23(5):1911–1919. https://doi.org/10.1109/JBHI.2018.2874033(2017)
17. Li H, Li A, Wang M (2019) A novel end-to-end brain tumor segmentation method using improved fully convolutional networks. Comput Biol Med 108:150–160. https://doi.org/10.1016/j.compbiomed.2019.03.014
18. Ronneberger O, Fischer P, Brox T (2015) U-Net: convolutional networks for biomedical image segmentation. In: Medical image computing and computer-assisted intervention (MICCAI), LNCS, vol 9351, pp 234–241, Springer. http://lmb.informatik.uni-freiburg.de/Publications/2015/RFB15a
19. Hu K, Gan Q, Zhang Y, Deng S, Xiao F, Huang W, Cao C, Gao X (2019) Brain tumor segmentation using multi-cascaded convolutional neural networks and conditional random field. IEEE Access 7:92615–92629. https://doi.org/10.1109/ACCESS.2019.2927433
20. Khan H, Shah PM, Shah MA, ul Islam S, Rodrigues JJ, (2020) Cascading handcrafted features and Convolutional Neural Network for IoT-enabled brain tumor segmentation. Comput Commun 153:196–207. https://doi.org/10.1016/j.comcom.2020.01.013
21. Wu W, Li D, Du J, Gao X, Gu W, Zhao F, Feng X, Yan H (2020) An intelligent diagnosis method of brain MRI tumor segmentation using deep convolutional neural network and SVM algorithm. Comput Math Methods Med 07(2020):1–10. https://doi.org/10.1155/2020/6789306
22. Chithra PL, Dheepa G (2020) Di-phase midway convolution and deconvolution network for brain tumor segmentation in MRI images. Int J Imaging Syst Technol 02:30. https://doi.org/10.1002/ima.22407
23. Zeineldin RA, Karar ME, Coburger J, Wirtz CR, Burgert O (2020) DeepSeg: deep neural network framework for automatic brain tumor segmentation using magnetic resonance FLAIR images. Int J CARS 15:909–920. https://doi.org/10.1007/s11548-020-02186-z
24. Simonyan K, Zisserman A (2015) Very deep convolutional networks for large-scale image recognition. International Conference on Learning Representations, 2015
25. He K, Zhang X, Ren S, Sun J (2016) Deep Residual Learning for Image Recognition. In: 2016 IEEE Conference on Computer Vision and Pattern Recognition (CVPR) p 770–778
26. Huang G, Liu Z, Maaten LVD, Weinberger KQ (2017) Densely connected convolutional networks. In: 2017 IEEE conference on computer vision and pattern recognition (CVPR) p 2261–2269
27. Chollet F (2017) Xception: Deep learning with depthwise separable convolutions. In: 2017 IEEE conference on computer vision and pattern recognition (CVPR) pp 1800–1807
28. Zoph B, Vasudevan V, Shlens J, Le QV (2018) Learning transferable architectures for scalable image recognition. In: Proceedings of the IEEE computer society conference on computer vision and pattern recognition, pp 8697–8710. https://doi.org/10.1109/CVPR.2018.00907
29. Sohail N, Anwar SM, Majeed F, Sanin C, Szczerbicki E (2021) Smart approach for glioma segmentation in magnetic resonance imaging using modified convolutional network architecture (U-NET). Cybern Syst 52:445–460. https://doi.org/10.1080/01969722.2020.1871231
30. Saeed MU, Al G, Bin W, Almotiri SH, AlGhamdi MA, Nagra AA, Masood K (2021) RMU-net: a novel residual mobile U-net model for brain tumor segmentation from MR images. Electronics 10:1962. https://doi.org/10.3390/electronics10161962
31. Sandler M, Howard A, Zhu M, Zhmoginov A, Chen LC (2018) MobileNetV2: inverted residuals and linear bottlenecks. In: IEEE/CVF conference on computer vision and pattern recognition (CVPR) pp 4510–4520. https://doi.org/10.1109/CVPR.2018.00474
32. Ozsahin I, Sekeroglu B, Mok GSP (2019) The use of back propagation neural networks and 18F-Florbetapir PET for early detection

of Alzheimer's disease using Alzheimer's Disease Neuroimaging Initiative database. PLoS ONE 14:1–13. https://doi.org/10.1371/journal.pone.0226577
33. Ozsahin I, Sekeroglu B, Pwavodi PC, Mok GSP (2020) High-accuracy Automated Diagnosis of Parkinson's Disease. Current Med Imaging, 16:6:688–694(7) https://doi.org/10.2174/1573405615666190620113607
34. Bakas S, Akbari H, Sotiras A, Bilello M, Rozycki M, Kirby JS, Freymann JB, Farahani K, Davatzikos C (2017) Advancing the cancer genome atlas glioma MRI collections with expert segmentation labels and radiomic features. Nat Sci Data 4:1–13. https://doi.org/10.1038/sdata.2017.117
35. Bakas S, Reyes M, Jakab A, Bauer S, Rempfler M, Crimi A et al (2018) Identifying the best machine learning algorithms for brain tumor segmentation, progression assessment, and overall survival prediction in the BRATS challenge. arXiv preprint arXiv:1811.02629
36. Bakas S, Akbari H, Sotiras A, Bilello M, Rozycki M, Kirby J, Freymann J, Farahani K, Davatzikos C (2017) Segmentation labels for the pre-operative scans of the TCGA-GBM collection. Cancer Imaging Archive. https://doi.org/10.7937/K9/TCIA.2017.KLXWJJ1Q
37. Bakas S, Akbari H, Sotiras A, Bilello M, Rozycki M, Kirby J, Freymann J, Farahani K, Davatzikos C (2017) Segmentation labels and radiomic features for the pre-operative scans of the TCGA-LGG collection. Cancer Imaging Archive. https://doi.org/10.7937/K9/TCIA.2017.GJQ7R0EF
38. Tania S, Rowaida R (2016) A Comparative Study of Various Image Filtering Techniques for Removing Various Noisy Pixels in Aerial Image. Int J Signal Process Image Process Pattern Recognit 9:113–124. https://doi.org/10.14257/ijsip.2016.9.3.10
39. Burger W, Burge MJ (2016) Digital image processing: an algorithmic introduction using Java. Springer-Verlag, Berlin
40. Allen M (2017) The SAGE encyclopedia of communication research methods. SAGE Publications, New York
41. Nai YH, Teo BW, Tan NL, O'Doherty S, Stephenson MC, Thian YL, Chiong E, Reilhac A (2021) Comparison of metrics for the evaluation of medical segmentations using prostate MRI dataset. Comput Biol Med 134:104497. https://doi.org/10.1016/j.compbiomed.2021.104497
42. Al-Antari MA, Al-Masni MA, Choi MT, Han SM, Kim TS (2018) A fully integrated computer-aided diagnosis system for digital X-ray mammograms via deep learning detection, segmentation, and classification. Int J Med Informatics 117:44–54. https://doi.org/10.1016/j.ijmedinf.2018.06.003
43. Wong TT (2015) Performance evaluation of classification algorithms by k-fold and leave-one-out cross validation. Pattern Recogn 48:2839–2846. https://doi.org/10.1016/j.patcog.2015.03.009
44. Montelius M, Ljungberg M, Horn M, Forssell-Aronsson E (2012) Tumour size measurement in a mouse model using high resolution MRI. BMC Med Imaging. https://doi.org/10.1186/1471-2342-12-12
45. Martinez-Murcia FJ, Gorriz JM, Ramirez J, Puntonet CG, Salas-Gonzalez D, Initiative Alzheimer's Disease Neuroimaging (2012) Computer aided diagnosis tool for Alzheimer's disease based on Mann-Whitney-Wilcoxon U-test. Expert Syst Appl 39:9676–9685. https://doi.org/10.1016/j.eswa.2012.02.153
46. Isensee F, Jaeger PF, Full PM, Vollmuth P, Maier-Hein KH (2021) nnU-Net for Brain Tumor Segmentation. In: Crimi A, Bakas S (eds) Brainlesion: glioma, multiple sclerosis, stroke and traumatic brain injuries. BrainLes 2020. Lecture notes in computer science, vol 12659. Springer, Cham. https://doi.org/10.1007/978-3-030-72087-2_11
47. Isensee F, Jaeger PF, Kohl SA, Petersen J, Maier-Hein KH (2021) nnU-Net: a self-configuring method for deep learning-based biomedical image segmentation. Nat Methods 18(2):203–211. https://doi.org/10.1038/s41592-020-01008-z
48. Jia H, Cai W, Huang H, Xia Y (2021) H2NF-net for brain tumor segmentation using multimodal MR imaging: 2nd place solution to BraTS challenge 2020 Segmentation Task. In: Crimi A, Bakas S (eds) Brainlesion: glioma, multiple sclerosis, stroke and traumatic brain injuries BrainLes 2020 Lecture notes in computer science, vol 12659. Springer, Cham. https://doi.org/10.1007/978-3-030-72087-2_6
49. Wang Y, Zhang Y, Hou F, Liu Y, Tian J, Zhong C, Zhang Y, He Z (2021) Modality-pairing learning for brain tumor segmentation. In: Crimi A, Bakas S (eds) Brainlesion: glioma, multiple sclerosis, stroke and traumatic brain injuries BrainLes 2020 Lecture notes in computer science, vol 12658. Springer, Cham. https://doi.org/10.1007/978-3-030-72084-1_21
50. Yuan Y (2021) Automatic brain tumor segmentation with scale attention network. In: Crimi A, Bakas S (eds) Brainlesion: glioma, multiple sclerosis, stroke and traumatic brain injuries. BrainLes 2020. Lecture notes in computer science, vol 12658. Springer, Cham. https://doi.org/10.1007/978-3-030-72084-1_26